Computational study of a label-free biosensor based on a photonic crystal nanocavity resonator

Saeed Olyaee* and Samira Najafgholinezhad

Nano-photonics and Optoelectronics Research Laboratory, Faculty of Electrical and Computer Engineering, Shahid Rajaee Teacher Training University (SRTTU), Tehran, Iran

*Corresponding author: s_olyaee@srttu.edu

Received 12 July 2013; revised 12 September 2013; accepted 25 September 2013; posted 26 September 2013 (Doc. ID 193767); published 10 October 2013

In this paper, we demonstrate and theoretically investigate a compact two-dimensional (2D) photonic crystal biosensor implemented by a waveguide and cavity. Biomaterials such as DNA molecules and proteins trapped inside a hole cause resonant wavelength shifting at the output terminal. The quality factor and sensitivity were obtained at about 4000 and 1.63 nm/fg, respectively. Also, we investigated this structure as a bulk refractive index sensor with a sensitivity of about 165.45 nm/RIU (refractive index units). Then, we modified the structure as a multichannel biosensor. This biosensor has the capability of highly parallel operation because of special architecture that was obtained by lattice shifting of a single hole around the cavity. Each channel had a different resonant cavity wavelength and the filling of analyte in selected holes caused resonant wavelength shifting, independently. Plane wave expansion (PWE) and finite difference time domain (FDTD) methods were used to analyze and compute the sensor characteristics.

OCIS codes: (280.1415) Biological sensing and sensors; (170.3890) Medical optics instrumentation; (160.1435) Biomaterials.

http://dx.doi.org/10.1364/AO.52.007206

1. Introduction

Photonic crystals are periodic dielectric materials in two or three directions that have the capability to manipulate light propagation. The introduction of a group of air pores into a silicon slab forms a forbidden frequency range, which is called the photonic band gap (PBG) [1–4]. Among all of the applications of photonic crystal structures, sensors for detecting vast numbers of physical properties have attracted the most attention [5–14]. By introducing defects in photonic crystals, locally confined optical states that are important for sensing applications emerge [15].

There are two basic sensing methods used with optical biosensors: fluorescent-based sensing and label-free sensing [16–19]. In the fluorescent method, first the target molecules are labeled by fluorescence and then the intensity of the fluorescence is used to represent the presence of molecules. In label-free detection, biomolecules are not labeled, but the mechanism of binding causes refractive index variation near the active sensing surface that can be used as a way to measure the concentration of biomolecules [20,21]. Photonic crystals based on the second method are utilized for measuring refractive index variation due to the high manipulation of light propagation.

By using defects such as micro or nanocavities based on photonic crystal resonators, various sensitive and high quality factor sensors can be achieved [22]. The photonic crystal structures are utilized for localizing strong fields within low refractive index holes, which makes the biosensor sensitive to refractive index changes. The presence of analyte inside the holes is detectable by measuring the output spectrum shift, especially when using micro and nanocavities with a high quality factor. The presence of a biochemical inside the selected holes, especially defects, causes spectral shifting that is monitored

1559-128X/13/297206-08$15.00/0

by a detector. The advantage of a nano/microcavity resonator is its smaller sensor area with a very small volume of analyte, which leads to locally strong light confinement and a high quality factor with better light–analyte interactions [23]. Direct-write dip-pen nanolithography (DPN), which can immobilize an analyte like DNA in a very small hole, is a sufficient technology for considering the single hole binding mechanism [24].

Dorfner *et al.* [25] have proposed a sensor with bulk refractive index sensing that has a sensitivity of about 103 nm/RIU (refractive index units) in the range of $n = 1$ to $n = 1.33$ with a detection limit (DL) of $2.4 \pm 0.1 \times 10^{-3}$ RIU. By investigating photonic crystal biosensors based on simulations, the design of structures with improved sensing properties can be achieved. For example, Passaro *et al.* [26] investigated a microstructure Bragg fiber as a biosensor for detecting the DNA hybridization process. A nanophotonic sensor based on a microcantilever that was integrated in a fluidic channel has been used to detect target molecules [27]. Lee and Fauchet [28] have demonstrated a biosensor based on a microcavity in a two-dimensional (2D) photonic crystal for protein and DNA molecules with a minimum detectable mass of about 2.5 fg. Hsiao and Lee [29] investigated a photonic crystal nanoring resonator as a biochemical sensor with a quality factor of about 2000. Then, in other work, they presented a biosensor with a Q-value of 3000 and a sensitivity of 0.5 nm/fg for DNA molecules and protein with a minimum detectable weight of 0.2 fg [22]. Dar *et al.* [30] have demonstrated a biosensor based on a ring resonator for DNA hybridization, theoretically. Similarly, in our research, the proposed structure was computationally studied. We applied a refractive index (RI) = 1.45 in our present research based on computational [22] and experimental [28] research done in photonic crystal biosensor analyses for DNA molecules.

Different methods, such as reducing or increasing the radius of selected holes, are used to create the cavity resonances [31]. However, in the present work, by omitting and displacing selected holes, a high quality factor and independent cavities in a single platform originated that were important for biomaterial detection.

In this paper, a 2D photonic crystal biosensor including the cavity and waveguide in a hexagonal lattice of holes in a silicon-on-insulator (SOI) slab is proposed. The target analyte that is trapped inside a single hole binds to bio-recognition molecules and because of this binding, the effective refractive index (ERI) of a selected hole is changed; as a result, the resonant wavelength shifts at the end of the waveguide, which is coupled via a cavity [32]. In this research, we designed the structure considering improved parameters. The proposed structure in both biosensing and refractive index sensing applications was investigated. Also, to overcome the single purpose performance of the sensor, a multichannel biosensor was designed. In Ref. [33], which is based on simulations, the results are shown for special refractive indices, such as $n = 1.5$, 1.75, 2, and 2.25 by introducing microcavities and waveguides. Displacing special holes in appropriate positions to select different resonant cavity structures in order to achieve new wavelengths is compatible with our purpose for designing a novel multichannel biosensor.

Mostly in this research, we focused on designing an ultra small size biosensor by studying both the physical design and parameter optimization using the approach of a single hole binding mechanism. By investigating these items in a compact structure, biomaterials in units of fentograms can be measured, which is a positive and remarkable feature of this work.

2. Materials and Methods

The structure of the photonic crystal with a hexagonal lattice is composed of a 230 nm thick layer of SOI wafer. The proposed structure shown in Fig. 1(a) was created by introducing line and point defects. The line and point defects were obtained by removing a group of holes and one hole, respectively. In this biosensor, the input of the waveguide was utilized for applying a Gaussian pulse in order to actuate the resonant mode of the cavity. Also, the output terminal was used for monitoring the trapped mode in order to calculate the quality factor and sensitivity [34].

The ERI and 2D finite difference time domain (FDTD) and plane wave expansion (PWE) approaches were used for analyzing this sensor. At first, the Gaussian pulse was applied to the input of the waveguide, and at the end of the waveguide, the output signal was recorded by a photodetector. Intonti *et al.* [35] demonstrated a spectral tuning mechanism for a photonic crystal microresonator wherein high quality resonators were rendered by flowing water within one or more holes around the cavity area. Consecutively, localized diversification of holes in the surface state with water in a 2D photonic crystal is technically feasible [35]. Also in biosensing applications, the presence of an aqueous surrounding is obtained by filling the entire surface of the structure with water in order to use this structure when it is embedded in a microfluidic channel. So in this structure, we considered that the holes were filled with water. The lattice constant and radius of the holes were 350 and 110 nm, respectively. The ERI of the dielectric and holes were considered as 2.825 and 1.33, respectively. The PBG for TE modes were obtained by the PWE method. According to Fig. 1(b), the PBG was in the range of 0.25455–0.3017.

3. Results and Discussion

A. Evaluation of Biosensing Characteristics

In this section, we demonstrate the structure analysis for biosensing applications based on a single hole binding mechanism. In biosensing applications, it is important to emphasize that the device cannot

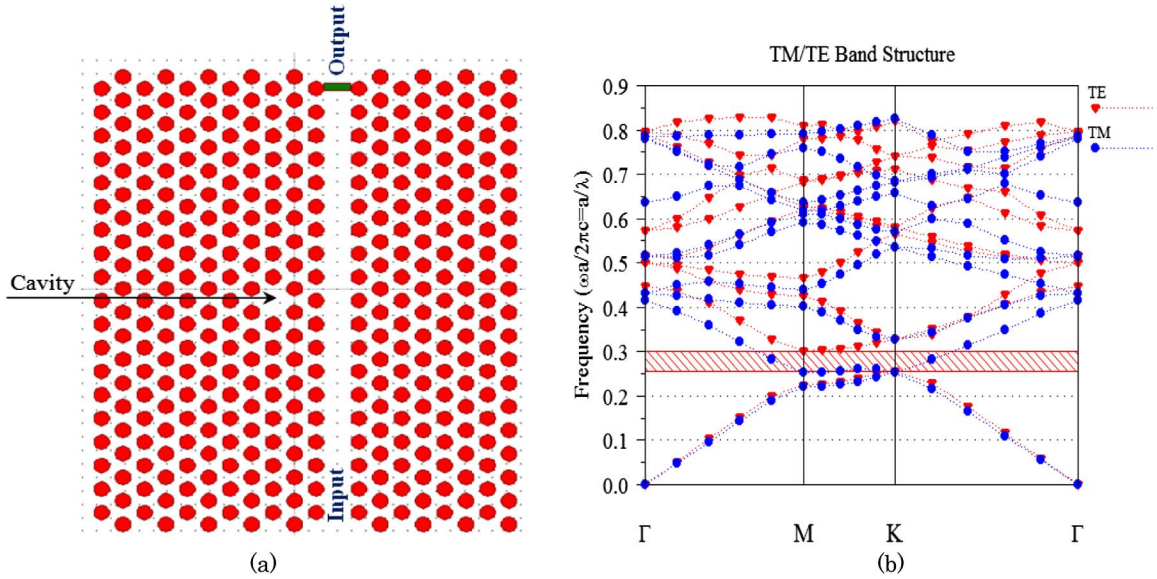

Fig. 1. 2D photonic crystal biosensor (a) structure and (b) band gap.

be utilized for measuring bulk refractive index variations around ambient conditions, whereas it can be used for measuring local refractive index variations. Hence, changing the RI of the hole around the cavity denotes that the target molecules bind to molecular probes, which have been predeposited [36]. Through the flowing of analyte within the sensing hole, the ERI of a selected hole is changed by the binding mechanism phenomenon. The binding mechanism is provided by an antigen and antibody, which traps the flowing analyte inside the selected hole. When the sensing hole is filled with this kind of material, the ERI is changed. Hence, the output spectrum can be obtained. As a result, spectral shifting is afforded because of ERI variations of the defect.

In this part, the structure has been optimized for obtaining a high quality factor and sensitivity. In the main structure where the holes are filled with water, the resonant wavelength is as shown in Fig. 2(a). Some holes around the cavity are labeled H_1, H_2, H_3, H_4, H_5, and H_6 in Fig. 2(b) and these were investigated by considering changes in the ERI. On the other hand, any of these holes can be considered as a hole that is filled by biomolecules. As mentioned, in this research the ERI of a hole that is completely filled by biomolecules is considered as $n = 1.45$.

The central wavelength, Q-value, wavelength shift, and $\Delta\lambda_{\mathrm{FWHM}}$ are listed for holes located around the cavity in Table 1, considering $n = 1.45$. According to Table 1, H_1, H_2, and H_3 have values that are approximately the same as H_6, H_5, and H_4, respectively, because of symmetry. As concluded from Table 1, H_1 could be selected as an optimized hole because of its high Q-value and sensitivity parameters. According to Table 1, the effect of the resonance wavelength shift and light confinement was mainly dominated by holes H_1 and H_6. In Fig. 3, the output spectrum of each hole around the cavity with its symmetric hole is shown for RI = 1.45. The data show that the output spectra of H_2 and H_3 are completely identical

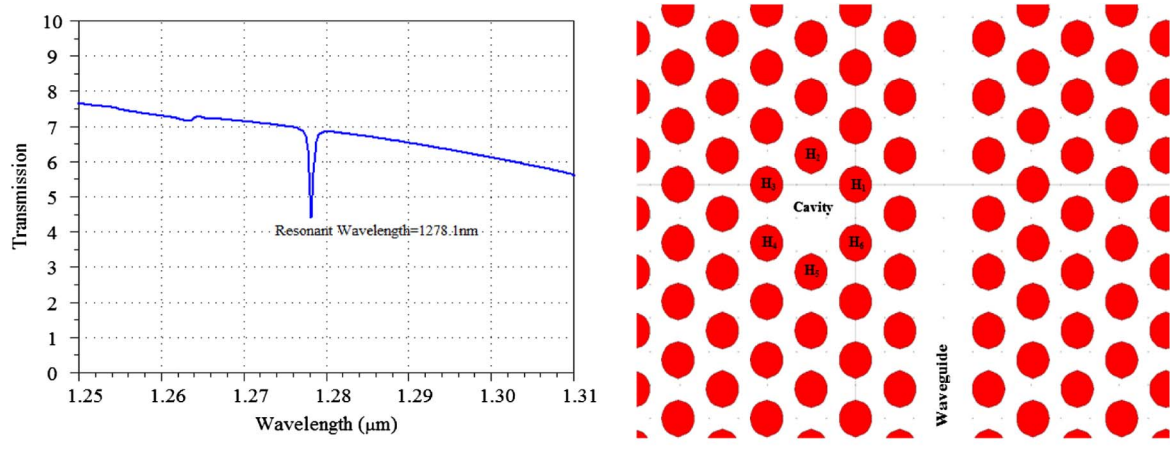

Fig. 2. (a) Transmission with respect to the wavelength and resonant wavelength of the photonic crystal biosensor and (b) layout of cavity and labeled holes around the cavity.

Table 1. Simulation Results of the Designed Biosensor for RI = 1.45

Sensing Hole	Wavelength Shift [nm]	Quality Factor	Resonant Wavelength [nm]	$\Delta\lambda_{FWHM}$ [nm]
Reference	0.0	4260.33	1278.1	0.3
H_1	2.2	4267.67	1280.3	0.3
H_2	0.4	4261.67	1278.5	0.3
H_3	0.9	2558.00	1279.0	0.5
H_4	0.9	2558.00	1279.0	0.5
H_5	0.4	4261.67	1278.5	0.3
H_6	2.2	3200.75	1280.3	0.4

with H_5 and H_4, respectively, which have the same Q-value and sensitivity. However, the output spectrum of hole H_1 was not completely identical with hole H_6. According to the results, H_6 had wider $\Delta\lambda_{FWHM}$ in comparison with its symmetric hole, which was caused by a coupling condition between the waveguide and cavity. The light is coupled from the waveguide to the cavity by holes located in the coupling distance. Hence, the hole H_6 is more exposed in the coupling path (light–analyte interaction) than hole H_1, and the group velocity ($\partial\omega/\partial k$) in H_6 is increased, which decreases the Q-value. In contrast, the other holes are not located in the coupling distance and just the coupled light is circulated in the cavity so that symmetric holes get the same portion of light.

In Fig. 4(a), the resonant wavelength shifts for H_1, H_2, and H_3 with a RI of $n = 1.45$ from the reference state (i.e., no analyte filled within the hole) are depicted. According to Fig. 4(a), H_1 showed a longer wavelength shift for $n = 1.45$ (and consequently more sensitivity) in comparison to the other holes.

In Fig. 4(b), the relation of refractive index variations and wavelength shifting is shown for three holes: H_1, H_2, and H_3 in the range of $n = 1.33$ to $n = 1.45$ with increments of 0.02. The slopes of the lines in Fig. 4(b) show the sensitivity. It can be concluded that the sensitivity and linearity for H_1 are larger than H_2 and H_3. Also in Table 2, we list the amount of resonant wavelength (λ_0) and its deviation from the reference state ($\Delta\lambda$) for H_1, H_2, and H_3.

The effect of coupling distance was also studied in our analyses. The change of coupling distance to 1, 2, or 3 periods revealed that with the increment of distance set to 3 periods, the quality factor increased but the sensitivity decreased; also, the output intensity was very low. Considering the distance to 1 period, the Q-value decreased and the sensitivity increased because of improved interactions of the analyte and light. Even with the obtained results, by considering 2 periods between the cavity and waveguide, we can achieve a reasonable Q-value and sensitivity that is depicted in our simulations.

According to the analysis done in the previous section for the designed structure, H_1 was selected as an optimized hole for a RI of $n = 1.45$ (DNA molecules), which had a high Q-value and sensitivity in

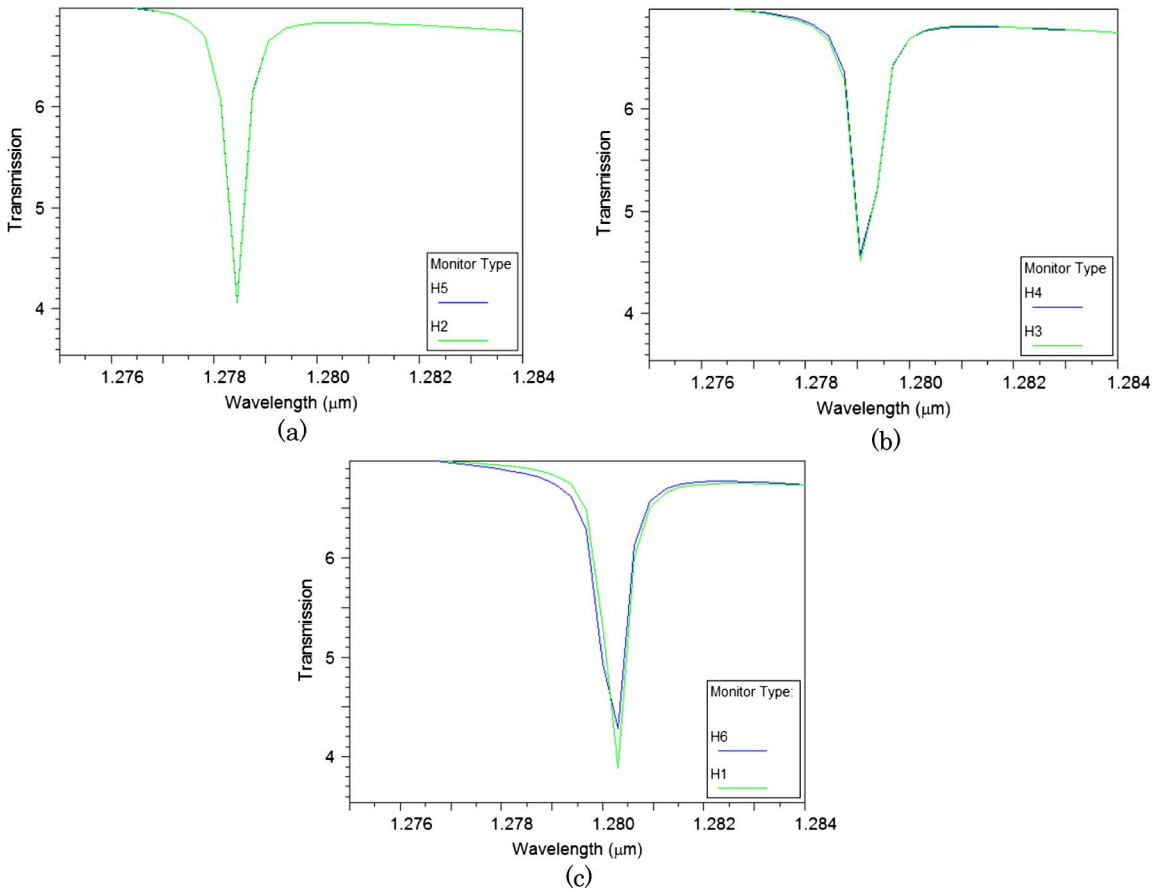

Fig. 3. Output spectrum of (a) H_2, (b) H_3, and (c) H_1 around the cavity with their symmetric holes for RI = 1.45.

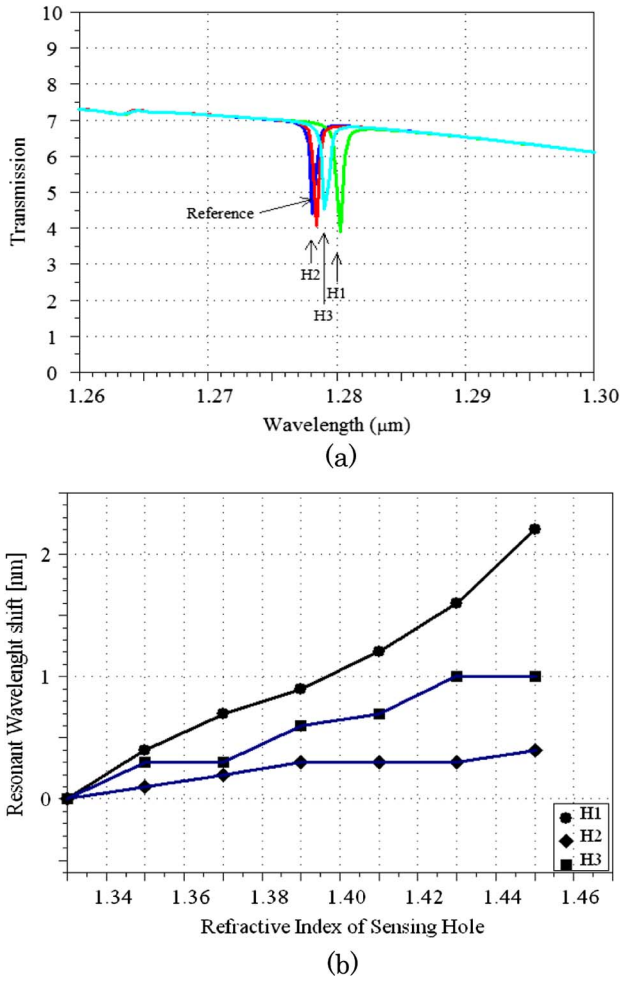

Fig. 4. (a) Transmission spectra of the designed biosensor with RI = 1.45 and (b) the resonant wavelength shift as a function of the refractive index in the range of 1.33–1.45 for three holes H_1, H_2, and H_3.

comparison with the other holes. When we suppose the ERI of a hole as $n = 1.45$, this means that the hole is filled completely by biomolecules. The average density of DNA molecules is 0.15 pg/μm^3 [22,37]. So in our structure, the obtained weight for DNA molecules will be 1.35 fg. The sensitivity, which is defined as the wavelength shift per the weight of the biomolecule in units of fentograms, is equal to $S = 1.63$ nm/fg ($\Delta\lambda = 2.2$ nm for $n = 1.45$). Now assuming the resolution of the measurement tools is 0.1 nm, the DL is 0.061 fg, which shows remarkable improvement in comparison to previous reports [22,28].

Table 2. Simulation Results for RI in the Range of $n = 1.33$ to $n = 1.45$ for Three Holes Around the Cavity

	λ_0 [nm] H_1	$\Delta\lambda$ [nm] H_1	λ_0 [nm] H_2	$\Delta\lambda$ [nm] H_2	λ_0 [nm] H_3	$\Delta\lambda$ [nm] H_3
$n = 1.33$	1278.1	0.0	1278.1	0.0	1278.1	0.0
$n = 1.35$	1278.5	0.4	1278.2	0.1	1278.4	0.3
$n = 1.37$	1278.8	0.7	1278.3	0.2	1278.4	0.3
$n = 1.39$	1279.0	0.9	1278.4	0.3	1278.7	0.6
$n = 1.41$	1279.3	1.2	1278.4	0.3	1278.8	0.7
$n = 1.43$	1279.9	1.6	1278.4	0.3	1279.1	1.0
$n = 1.45$	1280.3	2.2	1278.5	0.4	1279.1	1.0

B. Sensor Characteristics in Bulk Refractive Index Sensing

In order to investigate the optical properties of the designed structure in bulk refractive index sensing applications, we analyzed the simulation results with increasing the refractive index of holes from air ($n = 1$) to water ($n = 1.33$) or isopropanol (IPA) ($n = 1.377$). According to Fig. 5, increasing the refractive index of the holes shifts the resonant wavelength to a larger value. For $n = 1, 1.33$, and 1.377, we obtained $\lambda_{air} = 1223.5$ nm, $Q = 6117.5$, $\lambda_{water} = 1278.1$ nm, $Q = 4260.33$, and $\lambda_{IPA} = 1287.1$ nm, $Q = 3219$, respectively. Therefore, we can calculate the sensitivity that is defined as the wavelength shift per refractive index unit ($\Delta\lambda/\Delta n$). The values of sensitivity were 165.45 nm/RIU for refractive indices between $n = 1$–1.33 and 170.02 nm/RIU for $n = 1$–1.377.

The DL (Δn) between $n = 1$ and $n = 1.33$ for one linewidth ($\Delta\lambda = \lambda_{air}/Q_{air}$) was obtained as DL $= 1.2 \times 10^3$ RIU, which indicates an effective improvement in the sensitivity and DL compared to [25]. As a result, with the increment of holes in the refractive index, the resonant wavelength shifts to longer wavelengths but the Q-value decreases because of the reflectivity reduction that emerges from weaker vertical confinement.

C. Expanding Structure of the Multichannel Biosensor

Designing a multichannel biosensor is the purpose of this section. In contrast to other structures that can be utilized for sensing biomolecules with one specific refractive index in a certain time, the designed biosensor in this section can be used for sensing three specific refractive indices simultaneously.

By creating a new resonant cavity structure, we can achieve a new wavelength by displacing the defect hole in an appropriate position. In our design

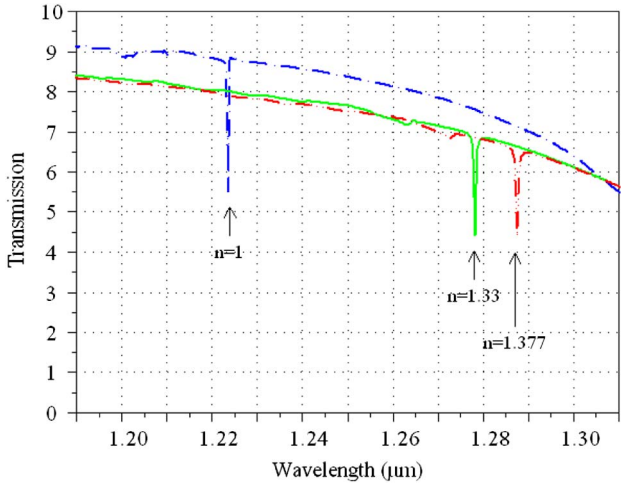

Fig. 5. Transmission spectra of the sensor in the refractive index sensing application.

of a multichannel biosensor, hole H_1 was shifted (d) in the direction shown in Fig. 6(a). The transmission spectrum resulting from the shift of d between 0 and 0.3 μm with increments of 0.05 μm is shown in Fig. 6(b). According to Fig. 6(c), after shifting the hole H_1 from 0 to 0.3 μm, the structure gave a new resonant wavelength. We used this feature to design a multichannel biosensor. As shown in Fig. 6(c), after $d = 0.1$ μm, the resonant wavelength was in linear proportion to d variations.

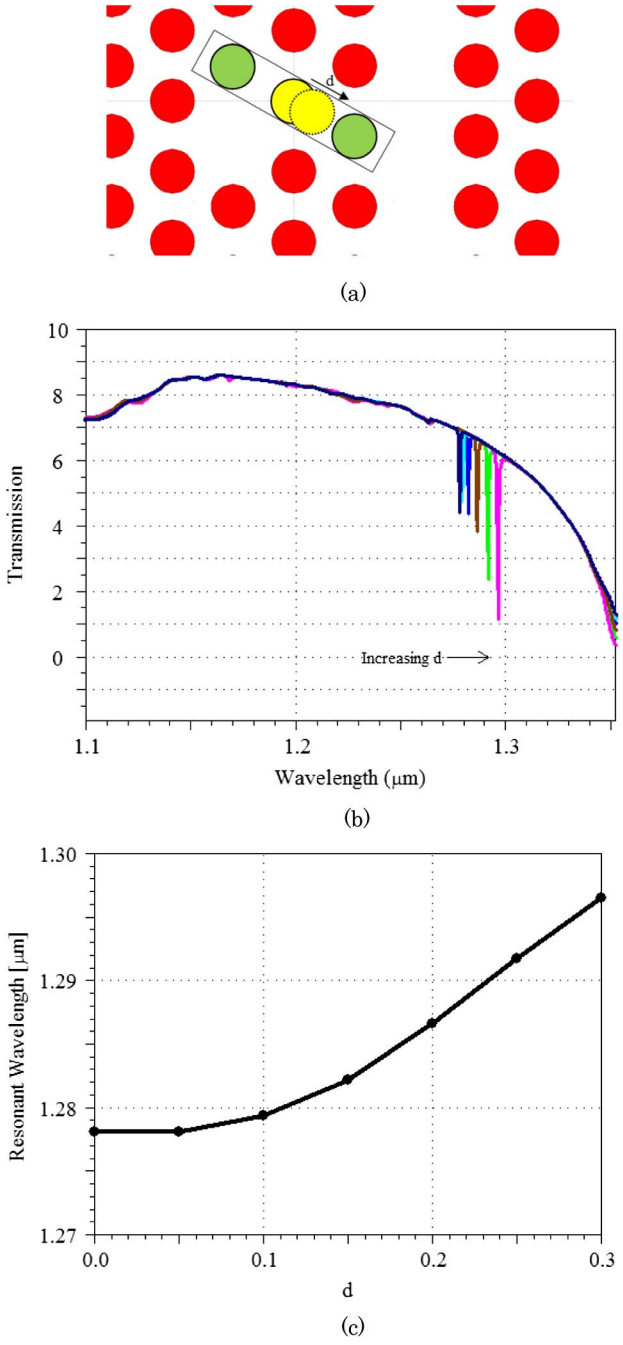

Fig. 6. (a) Layout of d variation and the effect of d variation on the (b) transmission spectra and (c) resonant wavelength in the range of 0–0.3 μm.

The designed biosensor shown in Fig. 7(a) was created by modifying three parts as follows. First, a row of holes was removed to create the main waveguide that was utilized for applying a Gaussian pulse, actuating the resonant modes of each cavity, and monitoring the output transmission. Then, three cavities were created by omitting some holes that were used for trapping special wavelengths, as shown in Fig. 7(a). Finally, hole H_1 was shifted slightly in the direction shown to design a new resonant cavity structure.

In channel 1, the cavity was obtained by omitting a hole. For channels 2 and 3, besides omitting a hole,

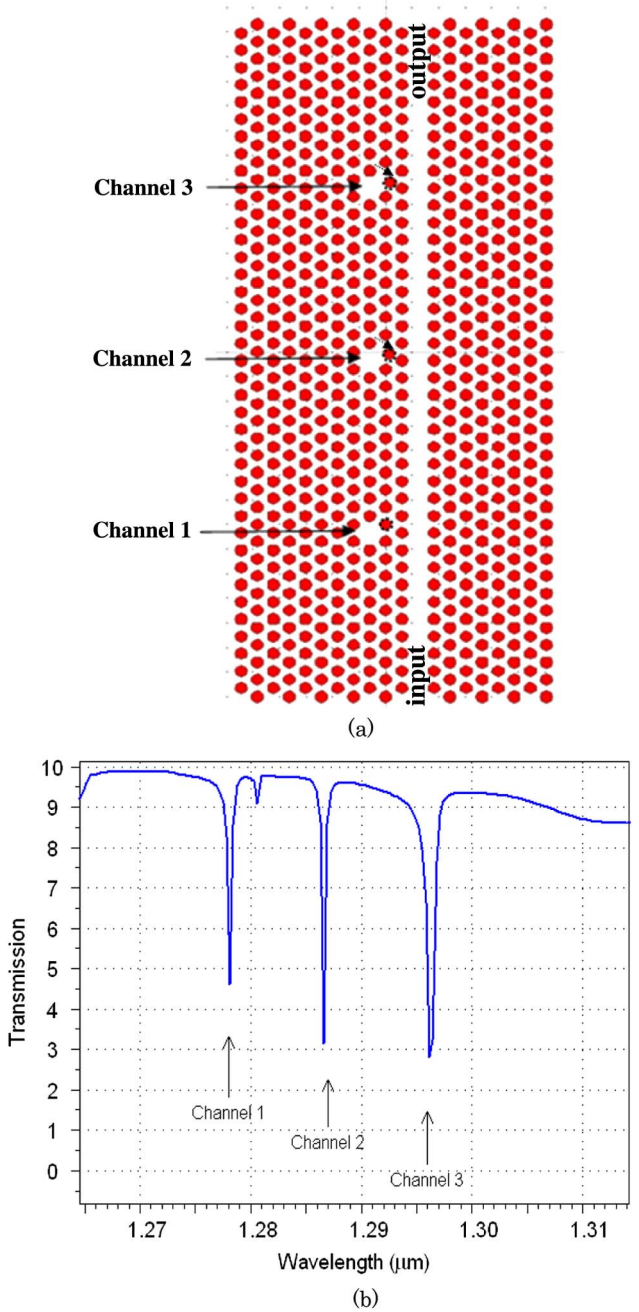

Fig. 7. (a) Structure and (b) transmission spectra of the designed multichannel biosensor.

lattice shifts of approximately 0.2 and 0.3 μm were applied, respectively, to create new channels. So for channels 2 and 3, the amount of d was 0.2 and 0.3 μm, respectively, to have enough channel wavelength spacing from each other. For channels 1, 2, and 3, the resonant wavelengths obtained were $\lambda_1 = 1.2781$ μm, $\lambda_2 = 1.2866$ μm, and $\lambda_3 = 1.2961$ μm, respectively [Fig. 7(b)]. It is obvious that the structure exhibited three narrow dips in the output transmission spectrum that were due to creation of three resonant cavities coupled to the waveguide. The quality factors for channels 1, 2, and 3 were 5000.0, 6433.0, and 2592.2, respectively. According to the analysis explained in the previous section for a single sensor structure, H_1 had been selected as an optimized hole for a RI of 1.33–1.45 because it had a high Q-value and sensitivity in comparison to the other holes. So in each new channel, H_1 is considered as the sensing hole.

A microfluidic system with incorporated microholes may be embedded in the designed biosensor structure to induct the analytes to the selected holes. When the analytes flow through these holes, the refractive indices of the holes are changed and the transmission spectra are varied. In order to validate the method of operation of the designed sensor, we show the effects of RI change from 1.33 to 1.45 for channel 3 in Fig. 8(a). Consequently, the resonant wavelength of channel 3 was changed, while the two others remained unchanged. According to the results, the refractive index variation of channel 3, which was caused by binding of the target with bio-recognition molecules, shifted the transmission spectrum to longer wavelengths. In Fig. 8(b), the dependency between the refractive index variation in the range of 1.33–1.45 and resonant wavelength shifting for channel 3 is depicted. In this range, the regression coefficient was 0.9961, which is indicative of good linearity.

By supposing an ERI for the hole of channel 3 as $n = 1.45$ for DNA molecules, the sensitivity and DL obtained were $S = 1.185$ nm/fg ($\Delta\lambda = 1.6$ nm for $n = 1.45$) and 0.084 fg, respectively, which showed improvement in respect to other reports such as the one by Hsiao and Lee [22].

According to Ref. [33], the results shown are for special refractive indices, such as $n = 1.5$, 1.75, 2, and 2.25. But in this paper, for increasing the usefulness of the designed device, the refractive index used in the simulation was as far as possible consistent with the refractive index of actual objects. Also, the designed microcavities in the above mentioned reference did not have independent resonant wavelengths. All of them had approximately the same resonant wavelengths. Because the resonant wavelengths were dependent with each other, the resolution of the calculations was reduced.

Guillermain and Fauchet [38] have designed and fabricated a double-channel sensor. In future work, we plan to fabricate our proposed structure and to compare the simulation and experimental results. The purpose of this paper was to design a novel

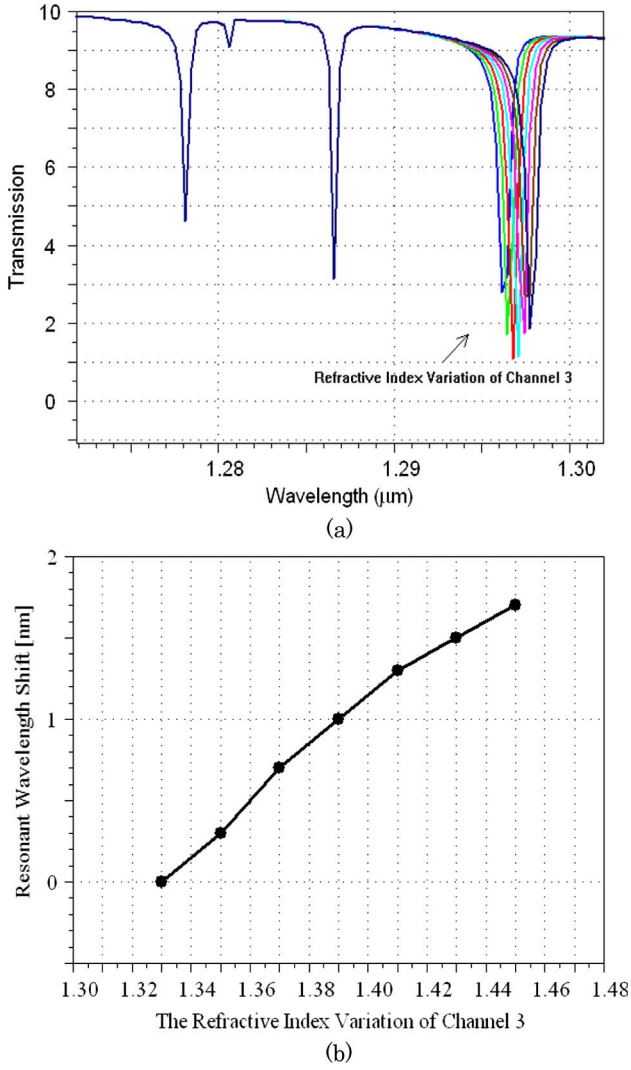

Fig. 8. (a) Transmission spectra and (b) resonant wavelength shift as a function of the refractive index in the range of 1.33–1.45 for channel 3 of the multichannel biosensor.

compact biosensor for measuring DNA molecules and to optimize the quality factor and sensitivity. Expanding the structure as a multichannel biosensor by displacing special holes in appropriate positions to select for different resonant cavity structures was investigated, and the results showed improved linearity. Additionally, the sensor had the capability of highly parallel operation because of its special architecture that was obtained by lattice shifting of the sensing hole around the cavity.

4. Conclusions

In this paper, we described a biosensor based on a 2D photonic crystal structure with a hexagonal lattice of holes in a SOI slab. The biosensor was obtained by introducing point and line defects. The structure was assumed to be embedded in a microfluidic channel and the holes filled with water. The biosensing mechanism was based on the ERI change of a single hole. Biomolecules like DNA and proteins filled in the special hole around the cavity cause ERI

variation of the hole because of the binding mechanism. Hence, the resonant wavelength in the output terminal shifts to a larger value. In this research, we achieved a quality factor of about 4000 and a sensitivity of 1.63 nm/fg, (the DL was 0.061 fg). The results showed that the resonance wavelength shifting and output intensity were dependent on the positions of the sensing holes. Also, this structure was investigated for use in bulk RI sensing. A sensitivity and DL of 165.45 nm/RIU and 1.2×10^{-3} RIU were obtained, respectively. To overcome the single purpose performance of the sensor and the amount of detected target molecules, a multichannel biosensor has been designed. The lattice shift of selected holes was an effective method to design a novel multichannel biosensor with a sensitivity of 1.185 nm/fg and a DL of 0.084 fg.

References

1. J. D. Joannopoulos, S. G. Johnson, J. N. Winn, and R. D. Meade, *Photonic Crystals: Molding the Flow of Light* (Princeton University, 2007).
2. J.-M. Lourtioz, "Photonic crystals and metamaterials," C. R. Physique **9**, 4–15 (2008).
3. J.-M. Lourtioz, H. Benisty, V. Berger, J.-M. Gerard, D. Maystre, and A. Tchelnokov, *Photonic Crystals: Towards Nanoscale Photonic Devices*, 2nd ed. (Springer, 2008).
4. S. Olyaee and F. Taghipour, "Ultra-flattened dispersion hexagonal photonic crystal fiber with low confinement loss and large effective area," IET Optoelectron. **6**, 82–87 (2012).
5. S. Olyaee and S. Najafgholinezhad, "A high quality factor and wide measurement range biosensor based on photonic crystal nanocavity resonator," Sens. Lett. **11**, 483–488 (2013).
6. Y. L. Hoo, W. Jin, C. Z. Shi, H. L. Ho, D. N. Wang, and S. C. Ruan, "Design and modeling of a photonic crystal fiber gas sensor," Appl. Opt. **42**, 3509–3515 (2003).
7. J. Sun and C. C. Chan, "Photonic bandgap fiber for refractive index measurement," Sens. Actuators B Chem. **128**, 46–50 (2007).
8. R. V. Nair and R. Vijaya, "Photonic crystal sensors: an overview," Prog. Quantum Electron. **34**, 89–134 (2010).
9. C. Lee and J. Thillaigovindan, "Optical nanomechanical sensor using Si photonic crystals cantilever embedded with nanocavity resonator," Appl. Opt. **48**, 1797–1803 (2009).
10. S. Olyaee and A. A. Dehghani, "High resolution and wide dynamic range pressure sensor based on two-dimensional photonic crystal," Photon. Sens. **2**, 92–96 (2012).
11. A. Säynätjoki, M. Mulot, K. Vynck, D. Cassagne, J. Ahopelto, and H. Lipsanen, "Properties, applications and fabrication of photonic crystals with ring-shaped holes in silicon-on-insulator," Photon. Nanostr. Fundam. Appl. **6**, 42–46 (2008).
12. S. Olyaee and A. A. Dehghani, "Nano-pressure sensor using high quality photonic crystal cavity resonator," in *IEEE, IET 8th International Symposium on Communication Systems, Networks and Digital Signal Processing* (CSNDSP, 2012), pp. 18–20.
13. S. Olyaee and A. A. Dehghani, "Ultrasensitive pressure sensor based on point defect resonant cavity in photonic crystal," Sens. Lett. (in press).
14. S. Olyaee, S. Najafgholinezhad, and H. Alipour Banaei, "Four-channel label-free photonic crystal biosensor using nanocavity resonators," Photon. Sens. **3**, 231–236 (2013).
15. A. Rostami, H. A. Banaei, F. Nazari, and A. Bahrami, "An ultra compact photonic crystal wavelength division demultiplexer using resonance cavities in a modified Y-branch structure," Optik **122**, 1481–1485 (2011).
16. P. C. Mathias, N. Ganesh, L. L. Chan, and B. T. Cunningham, "Combined enhanced fluorescence and label-free biomolecular detection with a photonic crystal surface," Appl. Opt. **46**, 2351–2360 (2007).
17. E. Hallynck and P. Biensman, "Photonic crystal biosensor based on angular spectrum analysis," Opt. Express **18**, 18164–18170 (2010).
18. W. Zhang, N. Ganesh, I. D. Block, and B. T. Cunningham, "High sensitivity photonic crystal biosensor incorporating nanorod structures for enhanced surface area," Sens. Actuators B Chem. **131**, 279–284 (2008).
19. J. Derbali, F. AbdelMalek, S. S. A. Obayya, H. Bouchriha, and R. Letizia, "Design of a compact photonic crystal sensor," Opt. Quantum Electron. **42**, 463–472 (2011).
20. X. Fan, I. M. White, S. I. Shopova, H. Zhu, J. D. Suter, and Y. Sun, "Sensitive optical biosensors for unlabeled targets: a review," Anal. Chim. Acta **620**, 8–26 (2008).
21. L. L. Chan, S. L. Gosangari, K. L. Watkin, and B. T. Cunningham, "A label-free photonic crystal biosensor imaging method for detection of cancer cell cytotoxicity and proliferation," Apoptosis **12**, 1061–1068 (2007).
22. F. Hsiao and Ch. Lee, "Computational study of photonic crystals nano-ring resonator for biochemical sensing," IEEE Sens. J. **10**, 1185–1191 (2010).
23. S. Blair and Y. Chen, "Resonant-enhanced evanescent-wave fluorescence biosensing with cylindrical optical cavities," Appl. Opt. **40**, 570–582 (2001).
24. S.-W. Chung, D. S. Ginger, M. W. Morales, Z. Zhang, V. Chandrasekhar, M. A. Ratner, and C. A. Mirkin, "Top-down meets bottom-up: dip-pen nanolithography and DNA-directed assembly of nanoscale electrical circuits," Small **1**, 64–69 (2005).
25. D. Dorfner, T. Zabel, T. Hürlimann, N. Hauke, L. Frandsen, U. Rant, G. Abstreiter, and J. Finley, "Photonic crystal nanostructures for optical biosensing applications," Biosens. Bioelectron. **24**, 3688–3692 (2009).
26. D. Passaro, M. Foroni, F. Poli, A. Cucinotta, S. Selleri, J. Lægsgaard, and A. Overgaard, "All-silica hollow-core microstructured Bragg fibers for biosensor application," IEEE Sens. J. **8**, 1280–1286 (2008).
27. W. Xiang and Ch. Lee, "Nanophotonics sensor based on microcantilever for chemical analysis," IEEE J. Sel. Top. Quantum Electron. **15**, 1323–1326 (2009).
28. M. R. Lee and P. M. Fauchet, "Two-dimensional silicon photonic crystal based biosensing platform for protein detection," Opt. Express **15**, 4530–4535 (2007).
29. F.-L. Hsiao and C. Lee, "Novel biosensor based on photonic crystal nano-ring resonator," Procedia Chem. **1**, 417–420 (2009).
30. T. Dar, J. Homola, B. M. Azizur Rahman, and M. Rajarajan, "Label-free slot-waveguide biosensor for the detection of DNA hybridization," Appl. Opt. **51**, 8195–8202 (2012).
31. S. Pal, E. Guillermain, R. Sriram, B. Miller, and P. M. Fauchet, "Microcavities in photonic crystal waveguides for biosensor applications," Proc. SPIE **7553**, 755304 (2010).
32. N. Skivesen, A. Tetu, M. Kristensen, J. Kjems, L. H. Frandsen, and P. I. Borel, "Photonic-crystal waveguide biosensor," Opt. Express **15**, 3169–3176 (2007).
33. M. Yun, Y. Wan, J. Liang, F. Xia, M. Liu, and L. Ren, "Multichannel biosensor based on photonic crystal waveguide and microcavities," Optik **123**, 1920–1922 (2012).
34. Y. Akahane, T. Asano, B. S. Song, and S. Noda, "High-Q photonic nanocavity in a two-dimensional photonic crystal," Nature **425**, 944–947 (2003).
35. F. Intonti, S. Vignolini, F. Riboli, M. Zani, D. S. Wiersma, L. Balet, L. H. Li, M. Francardi, A. Gerardino, A. Fiore, and M. Gurioli, "Tuning of photonic crystal cavities by controlled removal of locally infiltrated water," Appl. Phys. Lett. **95**, 173112 (2009).
36. D. Yang, H. Tian, and Y. Ji, "Nanoscale photonic crystal sensor arrays on monolithic substrates using side-coupled resonant cavity arrays," Opt. Express **19**, 20023–20034 (2011).
37. M. D. Bennett, J. S. Heslop-Harrison, J. B. Smith, and J. P. Ward, "DNA density in mitotic and meiotic metaphase chromosomes of plants and animals," J. Cell Sci. **63**, 173–179 (1983).
38. E. Guillermain and P. M. Fauchet, "Multi-channel biodetection via resonant microcavities coupled to a photonic crystal waveguide," Proc. SPIE **7167**, 71670D (2009).